Michael Zaiser*

# Statistical aspects of microplasticity: experiments, discrete dislocation simulations and stochastic continuum models

**Abstract:** The plastic deformation properties of microscale and nanoscale specimens differ from those of their macroscopic counterparts as the discrete nature of the elementary processes governing plastic flow becomes directly visible. In such specimens, details of the initial defect microstructure may exert a strong influence on the recorded deformation behaviour, which accordingly exhibits significant scatter even amongst specimens that share an identical preparation history. The plasticity of microsamples appears as a sequence of spatially and temporally localised events and not as the smooth and continuous flow process envisaged by classical continuum elastoplasticity. These observations pose a significant challenge to constitutive modelling. In this feature article, we discuss the statistics of fluctuations in microscale and nanoscale plasticity and discuss the implications for computational modelling of plastic deformation processes on microscale and nanoscales. We propose a new type of constitutive models that combine a classical continuum description of the elastic problem with a stochastic description of the dynamics of plastic flow.

**Keywords:** dislocations; fluctuations; plasticity.

***Corresponding author: Michael Zaiser,** School of Engineering, Institute for Materials and Processes, The King's Buildings, Sanderson Building, Edinburgh EH93JL, UK, e-mail: m.zaiser@ed.ac.uk
**M. Zaiser:** Institute for Materials Modelling, Department of Materials Science, University of Erlangen-Nürnberg, Dr.-Mack-Strasse 77, 90762 Fürth, Germany

## 1 Introduction

As a consequence of the progressive miniaturisation of systems and devices, classical questions of materials engineering such as the plastic deformation behaviour of crystalline and non-crystalline solids have to be addressed on smaller and smaller scales. Traditional concepts of materials plasticity – in principle, a well-established and settled field – have to be reassessed to decide whether they can meet the demands posed by the design and manufacturing of components as miniaturisation proceeds to microscales and nanoscales. Where changes in scale manifest qualitative changes in behaviour, a renewed effort in fundamental research is required to provide the conceptual and computational tools required for predicting and controlling the plastic deformation processes.

The plasticity of the samples with dimensions on the micrometer and submicrometer scale differs from macroscopic plasticity in two important respects: (i) the flow stress of small samples depends on their size ("smaller is stronger") and (ii) the scatter of plasticity data increases immensely, to the extent that the standard deviation of flow stress data is of the same order of magnitude as the mean flow stress. Both effects are illustrated in Figure 1 showing a series of deformation curves of molybdenum (Mo) nanopillars (for a description of the experiments, see [1,2]) together with a macroscopic deformation curve of the same material under comparable deformation conditions [3].

A large number of experimental and theoretical investigations have been devoted to the measurement and computational modelling of size effects in microplasticity (for recent reviews, see [4–6]). A significant theoretical effort has been devoted to models that retain the continuum framework while including length scales – which are absent from classical plasticity models – into constitutive equations for plasticity. Scale dependence of the constitutive equations as a necessary prerequisite for modelling size effects has been introduced either by nonlocal generalisations of plastic flow rules (non-local or gradient plasticity) [7–9] or, more recently, by recourse on fundamental physical mechanisms of dislocation motion that are cast into a continuum framework (continuum dislocation dynamics) [10–15]. An alternative approach is provided by discrete dislocation dynamics (DDD) simulations [16–19], but these are still confined to small systems/small strains and have difficulties in handling complex boundary conditions as encountered in problems of technological relevance.

By their nature, traditional continuum theories of plasticity make deterministic predictions and thus cannot address the issue of fluctuations. This is not a major

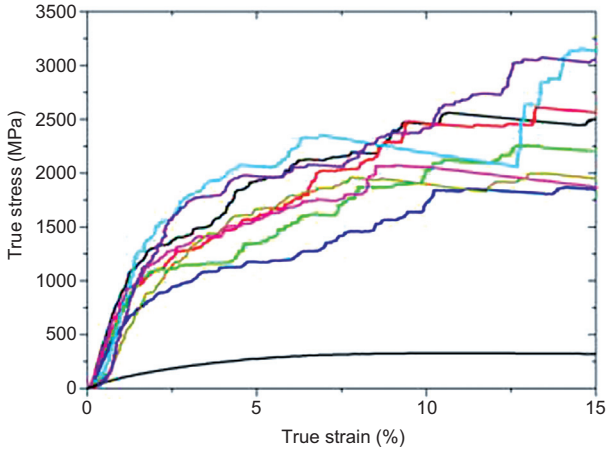


**Figure 1** Top, Stress-strain curves of [100]-oriented Mo micropillars, mean diameter $d$=0.3 μm [1, 2]. Bottom, Room temperature stress-strain curve of macroscopic [100]-oriented Mo single crystal (after Hollang et al. [3]).

problem in macroscopic plasticity because the scatter of deformation properties amongst different samples of a well-characterised material is small. However, fluctuations pose a major challenge for developing constitutive models in microplasticity, where even samples that have been machined from the same single crystal – as shown in Figure 1 – may exhibit a 50% scatter in flow stress. What is the use of predicting a mean flow stress of 1500 MPa at 5% strain when the scatter between different samples ranges between 1100 and 2200 MPa? A fundamental purpose of the scientific investigation of plastic deformation processes – on the microscale as well as on the macroscale – is to provide engineers with tools that allow them to predict the performance and reliability of components in technical systems. Unless the issue of "scatter" can be satisfactorily addressed, scientists will have failed in this task as far as microplasticity is concerned. We need to understand how the large fluctuations of microscale deformation behaviour that are consistently observed in simulations and experiments affect predictions of small-scale plasticity and how we can obtain reliability estimates for the deformation behaviour of microscale components.

What are the origins of scatter in microplasticity? Underlying the stress-strain curves, plasticity is governed by the (deterministic) dynamics of discrete objects, namely the interacting dislocation lines. These dynamics are inherently non-linear and characterised by collective phenomena, which can be broadly envisaged within the conceptual framework of non-equilibrium statistical mechanics and complexity theory [20]. Because of the complex nature of the underlying deterministic dynamics, small changes in initial conditions may lead to significant changes in deformation behaviour. As these changes are related to the local configuration of individual discrete defects, they can, in principle, not be captured within a deterministic continuum framework. Thus, to account for scatter in microplasticity, we either need to study the underlying discrete dynamics (perform discrete dislocation dynamics simulations for large strains and complex geometries) or we need to generalise continuum models to include local variability. In such models, our lack of knowledge regarding the local initial conditions and the inherently complex dynamics of dislocation systems need to be reflected by an appropriate stochastic description of the deformation process.

The aim is thus to replace the complex dynamics of interacting dislocations in the different volume elements of deforming crystals by equivalent spatiotemporal stochastic processes involving the continuum variables of stress, plastic strain, and possible internal variables. "Equivalent" must be understood here in a statistical sense: equivalence means that, over an ensemble of simulations, the relevant statistical characteristics of the overall deformation behaviour and of the internal stress and strain patterns are correctly reproduced.

There are, in principle, two strategies towards developing such a stochastic theory of microplasticity. We may statistically characterise experimental deformation curves [2] and surface deformation patterns [21–23], and we may use advanced strain mapping and imaging techniques to gain access to the statistics of internal stress and strain fields to deduce statistical characteristics of real deformation processes and obtain information required for constructing a matching stochastic description. This strategy is, however, limited by the practical difficulties of obtaining sufficiently large statistical ensembles of experimental data as required for a reliable statistical analysis. An alternative approach is provided by ensemble simulations of discrete dislocation dynamics. This has the advantage of giving direct access to stress and strain patterns on all scales above the atomistic scale and provides the additional possibility of assessing the relevance of various dislocation mechanisms and of different types of initial dislocation configurations by systematically varying respective parameters. In the remainder of this article, we will illustrate both approaches. Section 2 gives an overview of the analysis of data from microcompression experiments, whereas Section 3 details the analysis of simulation results obtained in compression and bending. Section 4 illustrates for a simple example how such results can be used for constructing a stochastic plasticity model and how such models can be used in a

Monte Carlo approach for assessing the possible outcomes of deformation processes.

## 2 Statistical analysis of microdeformation experiments

In the following, we illustrate the statistical analysis of microdeformation processes for the example of compression experiments conducted on Mo micropillars. We focus exclusively on the data analysis aspects; for a description of the experimental details, the reader is referred to the original articles [1, 2].

The deformation curves of compressed micropillars are characterised by a strongly intermittent behaviour: deformation proceeds as a discrete sequence of "deformation events", during which the plastic deformation rate increases significantly, and these events are separated by intervals of near-elastic stress increase. The shape of the corresponding stress-strain curves depends on the loading mode. On the one hand, in displacement-controlled deformation, rapid plastic flow during a deformation event leads to elastic unloading. Hence, the stress-strain curves assume a serrated shape where each deformation event corresponds to a stress drop. In stress-controlled loading, on the other hand, rapid deformation leads to a strain increase at almost constant stress. The corresponding, almost-horizontal parts of the stress-strain curve are separated by much steeper intervals of low plastic activity where the stress increases in a nearly elastic manner. Hence, the stress-strain curves assume a staircase-like shape, as seen in Figure 1. Both stress and strain increments scatter widely, leading to a variation in flow stresses that increases with increasing strain.

An obvious first step towards a statistical characterisation of deformation curves consists in determining the average value and the statistical variation of flow stresses as functions of strain and specimen size. This is shown in Figures 2 and 3. It can be seen that both the flow stress and the flow stress variation of Mo micropillars are size dependent. They rise rapidly at the onset of deformation and saturate above strains of about 10%.

Figure 4 demonstrates that the size-dependent flow stress and flow stress variation scale in approximate proportion with each other. Both dependences can be well described by inverse power laws, $\langle\sigma\rangle \sim \langle\Delta\sigma^2\rangle^{1/2} \sim d^{-a}$, where $a \approx 0.5$ and $d$ is the micropillar diameter.

For a more detailed statistical analysis, we consider the sequence of strain bursts and stress increases observed in stress-controlled compression tests. To analyse the

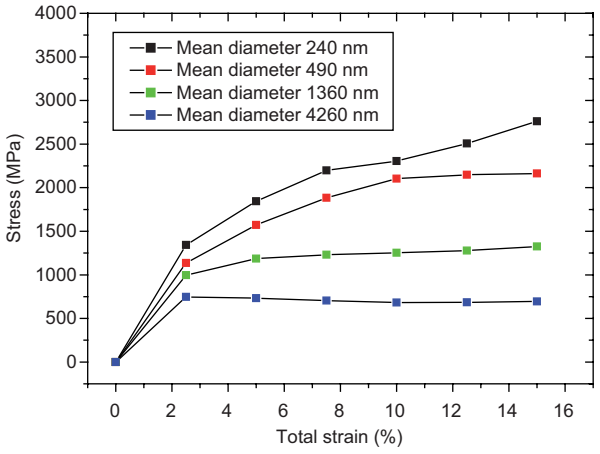


**Figure 2** Average deformation curves of Mo micropillars and nanopillars of different diameters. Each curve represents an average of eight samples. Data from [1, 2].

statistical properties of this sequence, we start out from time records of stress, plastic strain, and strain rate. After filtering out external sources of noise in the signals, we construct a sequence of deformation events by imposing a threshold on the plastic strain rate (for details, see [2]). The ensuing series of stress and strain jumps can be statistically characterised in terms of probability distributions of stress increments $\Delta\sigma$ and strain increments $\Delta\varepsilon$. The strain bursts exhibit a scale-free power law distribution:

$$p(\Delta\varepsilon) \propto \Delta\varepsilon^{-\kappa} \tag{1}$$

with an exponent $\kappa$ close to 3/2 as also reported for many other materials [20]. The distributions do not depend appreciably on system size (Figure 5). By contrast, the

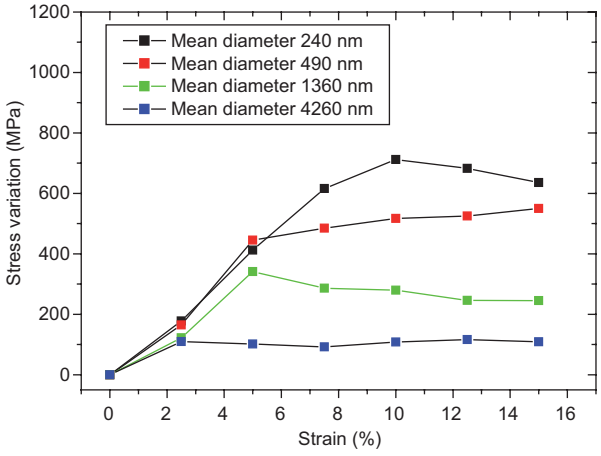


**Figure 3** Scatter of deformation curves of Mo micropillars and nanopillars of different diameters. Each curve represents the standard deviation of the flow stresses of eight samples. Data from [1, 2].

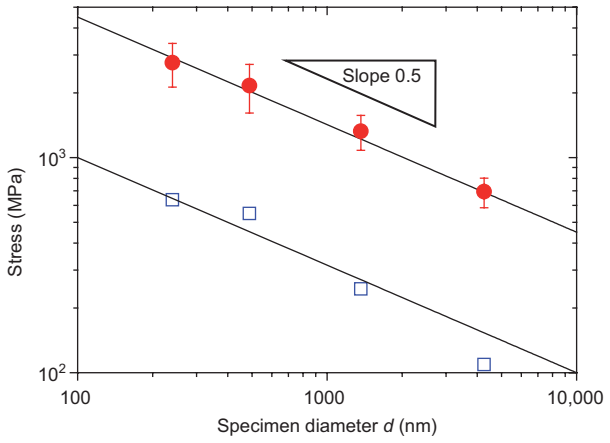


**Figure 4** Size dependence of the flow stress and flow stress variation of [100]-oriented Mo single crystals (both parameters determined at 15% strain).

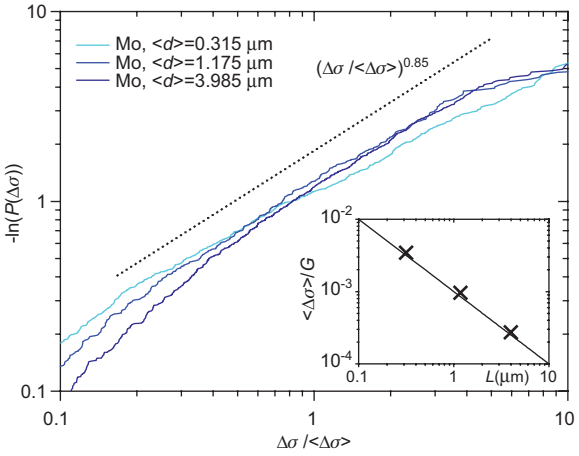


**Figure 6** Cumulative probability distributions of stress increments determined in stress-controlled compression of [100]-oriented Mo micropillars of different sizes. The straight line is a Weibull distribution with parameter 0.87. Inset, Mean stress increment as a function of sample diameter.

distributions of stress increments show a clear system size dependence (Figure 6). They are not scale-free – in fact, they can be represented well by Weibull distributions,

$$p(\Delta\sigma) \propto \frac{1}{\beta}\left(\frac{\Delta\sigma}{\Delta\sigma_0}\right)^{\beta-1} \exp\left[-\left(\frac{\Delta\sigma}{\Delta\sigma_0}\right)^{\beta}\right] \qquad (2)$$

with a shape parameter (Weibull exponent) $\beta$ close to 1, i.e., we find near-exponential behaviour. This parameter does not depend on the system size. The mean stress increment (and also the stress parameter $\Delta\sigma_0$ of the Weibull distributions), by contrast, is inversely proportional to the system size (inset in Figure 6). This poses the question how the size dependences of the flow stress and of the stress increment distribution relate to each other.

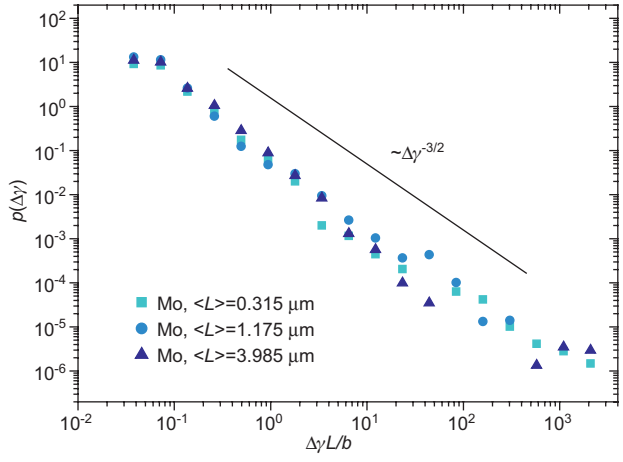


**Figure 5** Probability distribution of strain increments determined in stress-controlled compression of [100]-oriented Mo micropillars of different sizes. The straight line indicates a power law distribution with exponent 3/2.

Before we address this question, a word of caution is needed. It is in the nature of power-law distributions with exponents between 1 and 2 that $p(\Delta\varepsilon)$ contains a very large number of small jumps as the probability density diverges at small $\Delta\varepsilon$. This "infrared divergence" must be mitigated by introducing a cut-off $\Delta\varepsilon_{min}$ at small sizes. The actual value of $\Delta\varepsilon_{min}$ is at first glance of little importance, as a simple calculation demonstrates that, for small $\Delta\varepsilon_{min}$, the (infinitely many) small events that are cut out produce only a negligible fraction of the overall strain. However, the value of the cut-off in the strain increment distribution is of crucial importance for the distribution of stress increments: it is evident that the mean stress increment simply equals the mean flow stress divided by the number of events that have occurred up to that stress. Reducing $\Delta\varepsilon_{min}$ (the smallest strain increment still counted as a strain jump) increases the number of events and hence reduces the mean value of the stress increment distribution. Thus, any discussion of the size dependence of the stress increment statistics is meaningless unless we specify how we define $\Delta\varepsilon_{min}$.

In our analysis of Mo micropillar deformation, the smallest event size was implicitly defined to be inversely proportional to the system size (the imposed requirement was that the corresponding displacement increment had to exceed the typical level of machine-induced oscillations in the displacement record). Using the relation $\Delta\varepsilon_{min} \sim d^{-1}$,

we may now try to understand the relation between the size dependence of the flow stress and the stress increment statistics.

To this end, we formulate a minimal statistical model by assuming that the stress and strain increments in a sequence are mutually uncorrelated random variables. In addition, we assume that the sequences of stress and strain increments constitute two independent, stationary stochastic processes such that the statistics of deformation curves is completely characterised by the respective probability distributions. Under these assumptions, the following statistical arguments can be put forward:

– The total number of events is equal to the total strain divided by the average strain increment:

$$N=\frac{\varepsilon}{\langle\Delta\varepsilon\rangle} \tag{3}$$

– For a power law distribution of exponent 3/2, the average is the arithmetic mean of the upper and lower cut-offs of the power law scaling regime. Hence, the average strain increment is

$$<\Delta\varepsilon> \propto \Delta\varepsilon_{\min}\Delta\varepsilon_{\max} \tag{4}$$

– The upper cut-off of the scaling regime is given by the total strain (at strain $\varepsilon$, no event with $\Delta\varepsilon>\varepsilon$ can possibly have occurred):

$$\Delta\varepsilon_{\max}\sim\varepsilon.$$

The average stress increment is given by the flow stress (determined at strain $\gamma$) divided by the number of strain increments that have occurred up to that strain:

$$\langle\Delta\sigma\rangle=\frac{\sigma}{N}=\frac{\sigma\langle\Delta\varepsilon\rangle}{\gamma}\propto\sigma\left(\frac{\Delta\varepsilon_{\min}}{\varepsilon}\right)^{1/2} \tag{5}$$

The analysis of flow stresses for the Mo experiments indicates that $\sigma\sim d^{1/2}$. Furthermore, $\Delta\varepsilon_{\min}\sim d^{1}$ due to the manner the stress-strain curves were analysed [2]. Inserting both relations into Eq. (5), we find that $<\Delta\sigma>\sim d^{1}$ as observed. Thus, the observed size dependences of the stress and stress increment statistics are mutually consistent within the framework of our minimal statistical model.

Temporal intermittency of microscale plasticity goes along with spatial localisation as the sequence of distinct deformation events corresponds to a pattern of localised slip bands. Using surface analysis methods, Schwerdtfeger et al. [22, 23] demonstrated that the local strains in slip bands obey the same statistics as the temporal strain increments during strain bursts, supporting the conjecture that each strain burst corresponds to the formation of a localised slip band. Although the slip band heights were demonstrated to exhibit scale-free statistics, the slip band spacings were exponentially distributed, supporting the idea that slip band nucleation can be envisaged as an uncorrelated Poisson process. Using these ideas, a statistical model of the formation and evolution of slip band patterns was proposed in [23], which produced a good agreement with the overall surface morphology observed in experiments on alkali halide single crystals.

Unfortunately, despite these successes, it is difficult to build statistical models of microplasticity exclusively upon experimental data. For evident reasons, experimentators shun the boring task of preparing and testing large numbers of identical specimens. Even in a carefully conducted and well-documented series of experiments, it is rare to find statistics based upon more than a dozen specimens for each set of physical and geometrical parameters. Moreover, it is difficult to fully characterise and reproduce – let alone independently control – the statistical parameters of the initial dislocation microstructure in different samples. As a consequence of incomplete characterisation and poor statistics, there is little agreement as to the physical origin of fluctuations and size effects. Even for a seemingly straightforward parameter as the size effect exponent $a$, different leading groups keep advocating different values (compare, e.g., the reviews [4, 6]). To overcome the difficulties related to poor statistics and insufficient information regarding microstructures, it is useful to resort to discrete dislocation dynamics simulations. Although such simulations have problems of their own (restriction to small samples and small strains), they allow to independently control the initial dislocation microstructure and simulate reasonably large ensembles by unsophisticated "farming out" of computations over multiple computers.

## 3 Statistical analysis of discrete dislocation dynamics simulations

To illustrate the statistical analysis of DDD simulations, we refer to simulations of microbending by Motz et al. [24] and, for comparison, to simulations of micropillar compression by Csikor et al. [25]. Again we discuss mainly the statistical analysis of stress-strain and dislocation density vs. strain curves. For details of the DDD method and specific parameters, the reader is referred to the original works.

The bending of Al microbeams was simulated by prescribing displacements on the end surfaces of

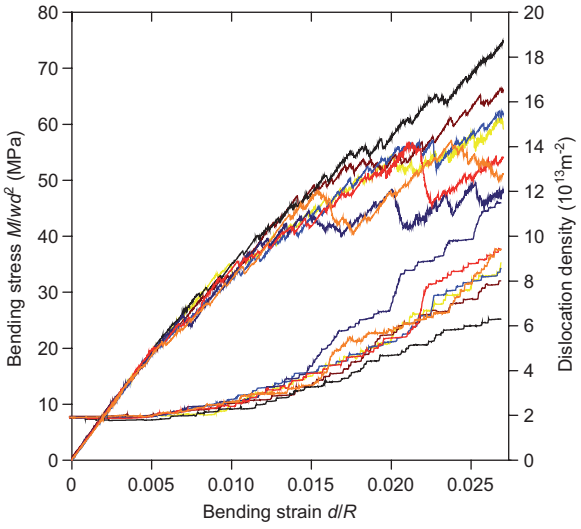


**Figure 7** Discrete dislocation dynamics simulations of microbending. Upper curves, scaled bending moment vs. total surface strain; lower curves, dislocation density vs. surface strain; [100]-oriented Al single crystals, specimen dimensions 0.75×0.75×1.5 μm.

[100]-oriented fcc single crystals with dimensions of 0.75×0.75×1.5 μm$^3$. The initial dislocation microstructure consisted of randomly distributed dislocation sources. The initial dislocation density was $2\times10^{13}$ m$^{-2}$, and the source length was chosen equal to the mean dislocation spacing. A bending strain rate of $2\times10^4$ s$^{-1}$ was imposed by keeping one end surface of the specimen fixed and displacing the other end surface to impose a given bending radius $R$. A set of resulting bending curves (bending moment vs. total surface strain) is shown in Figure 7 together with the corresponding dislocation density vs. strain records.

Figure 8 demonstrates the correlation between the stress and dislocation density evolution and the strain rate vs. time record. It can be seen that each strain burst corresponds to a drop in bending moment and a simultaneous upward jump in dislocation density. This is due to the strain gradient in the microbending test, which neccessitates the accumulation of geometrically necessary dislocations (GNDs) during plastic deformation. In view of the theoretical interpretation of microbending size effects, it is interesting to take a look at the sample-to-sample variations of stress and dislocation density evolution. From Figure 7, it is seen quite clearly that the samples that deform plastically at the lowest bending moment are those that exhibit the largest accumulation of dislocations. This finding is consistent with the concept of plastic strain gradients causing GND accumulation but difficult to reconcile with the popular idea (see, e.g., [8]) that a larger GND density supposedly leads to a higher flow stress, causing a size effect. Figure 9 shows, for comparison, the same records for a uniaxial compression test. Here, again, there is a clear correlation between stress drops and strain bursts. However, the strain bursts are, in this case, not associated with any appreciable changes in dislocation density, thus refuting the idea that strain bursts might be associated with either rapid dislocation multiplication or dislocation depletion through the specimen surfaces.

We now proceed to statistically analyse the evolution of stress, strain, and dislocation density. To this end, we determine the statistics of plastic strain and dislocation density increments associated with strain bursts, as well as the stress changes between bursts. We smoothen the simulated strain rate vs. time signals by performing a running average over a short time interval to eliminate high-frequency strain rate oscillations associated with the discretisation of dislocation lines and then threshold the smoothened signal to identify "strain bursts" as time intervals over which the strain rate continuously exceeds

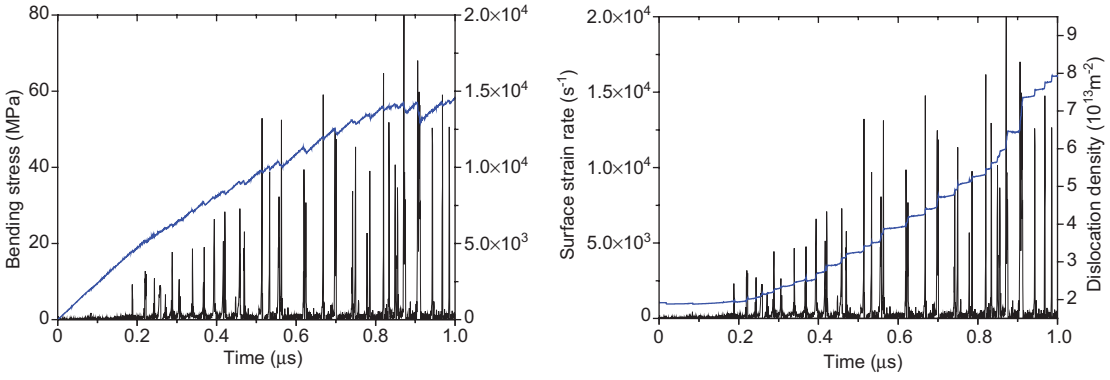


**Figure 8** Stress, strain rate, and dislocation density vs. time signals in a DDD simulation of microbending. Left, Scaled bending moment vs. time and plastic surface strain rate vs. time; right, dislocation density vs. time and plastic surface strain rate vs. time.

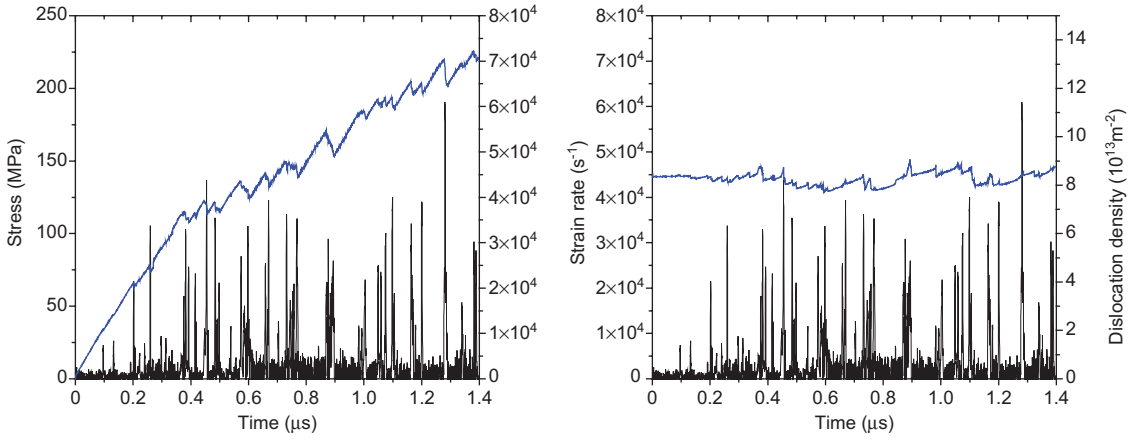


**Figure 9** Stress, strain rate, and dislocation density vs. time signals in a DDD simulation of uniaxial compression. Left, Stress vs. time and strain rate vs. time; right, dislocation density vs. time and strain rate vs. time.

the imposed threshold value. Strain and dislocation density increments are then simply defined as the differences between the values of plastic strain and total dislocation density at the start and the end of the burst.

Figure 10 demonstrates the near-perfect agreement between the distributions of dislocation density increments and strain burst sizes. Both variables appear to be linked by the simple linear relationship $K\Delta\varepsilon=\Delta\rho$, where the value $K\sim10^{17}$ m$^{-2}$ compares well with the minimal proportionality factor that follows from geometrical considerations for GNDs, $K=1/(b_\perp d)=7.5\times10^{16}$, where $b_\perp=1.77\times10^{-10}$ m is the projection length of the Burgers vector on the [100] axis and $d=0.75\times10^{-6}$ m is the specimen thickness.

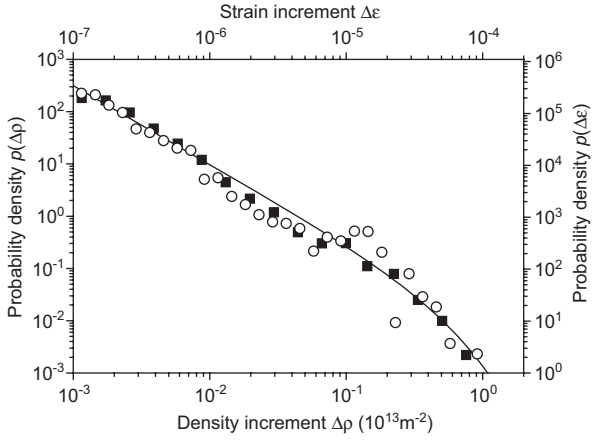


**Figure 10** Distributions of strain and dislocation density increments in discrete dislocation dynamics simulations of microbending. The corresponding stress-strain and dislocation density vs. strain curves are shown in Figure 7/Full line, Truncated power law [cf. Eq. (6)].

If we compare these results with those obtained for displacement-controlled uniaxial deformation simulations (see Figure 11, which compiles strain increment distributions from bending, uniaxial deformation, and experiment), we make the surprising observation that the strain increments follow in both cases the same distribution, whereas the dislocation density increments in uniaxial deformation are much smaller, have zero average, and show no indication of scale-free behaviour. This leads to the surprising conclusion that the very significant accumulation of GNDs in the bending simulations has little impact on the strain burst phenomenon, which thus seems to be quite insensitive to the presence or absence of strain gradients. Irrespective of deformation mode and material parameters, the distribution of strain burst sizes (strain increments) appears to be well described by a truncated power law,

$$p(\Delta\varepsilon)=N\Delta\varepsilon^{-3/2}\exp\left[-\frac{\Delta\varepsilon}{\Delta\varepsilon_{\max}}\right],\ \Delta\varepsilon_{\max}=\frac{Eb}{(\Theta+M)l} \qquad (6)$$

where $N$ is a normalisation constant. The cut-off $\Delta\varepsilon_{\max}$ is found to be inversely proportional to the system size $l$ and to the sum of the intrinsic hardening coefficient $\Theta$ and a stiffness parameter $M$. The latter parameter governs the stress reduction in response to a plastic strain increment in conditions of displacement control; it is equal to zero in stress-controlled experiments and is equal to the elastic modulus $E$ for displacement-controlled deformation with an ideally stiff machine. Relation (6) was first found in simulations of a stochastic microplasticity model by Zaiser and Nikitas [26], and the scaling $\Delta\varepsilon_{\max}\sim1/l$ was later confirmed for a generic dislocation-based model by

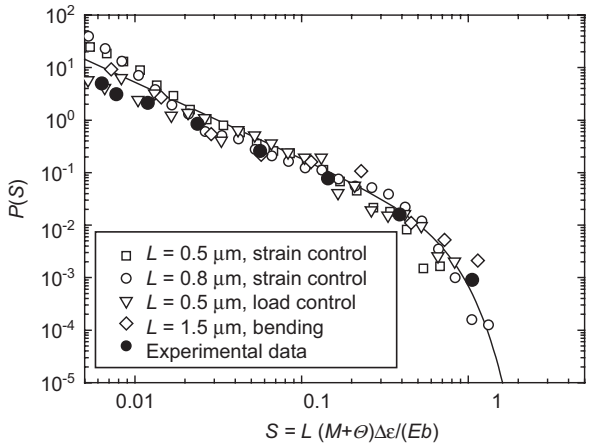


**Figure 11** Comparison of the statistics of strain burst sizes in microcompression and microbending simulations and in micropillar compression experiments [25]. Full line, Fit according to Eq. (6).

Salman and Truskinovsky [27], as well as by discrete dislocation dynamics simulations [25].

We now turn to the statistics of stress increments between strain bursts. We define the stress increment between two bursts as the difference of the stresses at burst initiation. In displacement-controlled deformation, we may thus observe negative stress increments. We exclude the first stress increments in each sequence, which correspond to the regime of elastic loading before yield.

The resulting stress increment distribution for our set of bending simulations is shown in Figure 12. The distribution consists of two regimes. First, we observe a regime

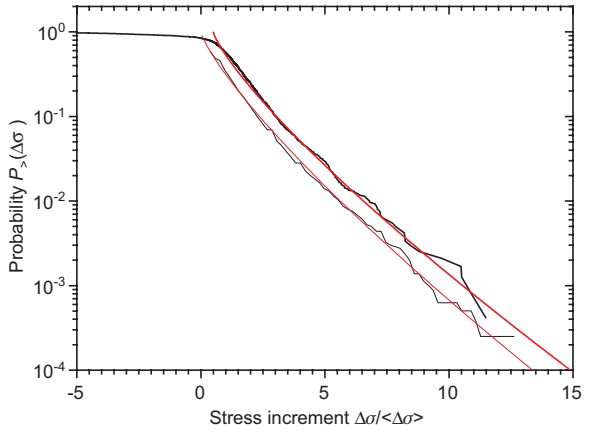


**Figure 12** Distribution of stress increments between strain bursts in discrete dislocation simulations of microbending (upper curve) and compression (lower curve; the red lines correspond to Weibull distributions) (modulus $\beta$=0.8).

of negative stress increments that have low overall probability ($P(\Delta\sigma<0)<0.1$), indicating that each strain burst tends to initiate at a higher stress than the preceding one. The bulk of the distribution at positive stress increments can be well described by a Weibull distribution of shape parameter $\beta$=0.8, similar to what we find in experiments (Section 3) and also in simulations of uniaxial deformation (see Figure 12).

In conclusion of this section, we note that there is a remarkable degree of similarity in the statistics of stress-strain curves obtained in simulated microbending and microcompression. This indicates universality of the mechanisms underlying strain bursts and fluctuation phenomena in microplasticity in general [20]. This universality, if it can be further corroborated, gives hope that it may be possible to develop generic models that allow to assess and evaluate the scatter of microdeformation processes. The structure and possible output of such models will be outlined in the following section.

# 4 Stochastic continuum modelling of microplasticity

As stated in the introduction, the ultimate aim of stochastic microplasticity models is to map the complex dynamics of interacting dislocations in the different volume elements of a deforming crystal onto equivalent spatiotemporal stochastic processes involving the continuum variables of stress and plastic strain. Using statistical information extracted from discrete dislocation dynamics simulations and/or experiments, we want to construct stochastic models that reproduce the essential statistical features of the deformation processes in small volumes of a material. The task is then to assemble these small volumes into larger samples in such a manner that the deformation of these samples is captured correctly.

To this end, interactions between the different volume elements need to be represented correctly. These interactions may conceptually be split into surface-mediated, short-range interactions that arise from the exchange of dislocations across the boundaries between adjacent volume elements and long-range interactions that emerge from the internal stresses that are required to maintain compatibility of deformation as the plastic flow of the individual volume elements proceeds in a heterogeneous and erratic manner. One the one hand, these long-range interactions arise naturally as we assemble elements with different stochastic deformation curves into a composite and can be captured by standard finite element calculations.

Surface-mediated interactions (dislocation exchange), on the other hand, can be related to imbalances in dislocation fluxes and hence to strain gradients. In a continuum setting, these interactions can be represented by gradient-dependent terms in the local flow rule as discussed by Zaiser and Aifantis [28, 29]. Besides providing a summary representation of dislocation fluxes and the associated internal length scales, these terms have an important role in computational modeling: as we refine the spatial resolution of a stochastic model, the relative fluctuations in deformation behaviour are bound to increase, leading to mesh-dependent and, in the continuum limit of infinite spatial resolution, non-differentiable strain patterns. Gradient terms in the flow rule fulfill the important role of suppressing short-wavelength fluctuations of the deformation fields and thus ensuring mesh independence of simulation results.

In the following, we illustrate the stochastic simulation of microdeformation processes on a particularly simple example, namely, the stress-controlled bending of a long thin rod of length $L$ and diameter $d$. The rod is clamped at one end and bent by applying a monotonically increasing torque to its other end. The simulation is terminated once this end has rotated by 180°, at which point – assuming the classical plasticity theory with an arbitrary monotonic hardening law – the rod should have bent into a circle. The geometry of a long thin rod is particularly convenient because such a rod can be envisaged as a sequence of segments where both short- and long-range interactions between different segments can be neglected. Furthermore, with the imposed boundary conditions, the solution of the elastic problem is trivial: the bending moment is constant along the rod and equals the applied torque. Thus, the rod can be envisaged as a sequence of (approximately) non-interacting segments deforming in series under the same applied stress that is controlled externally. As a consequence, the overall deformation of the rod can be calculated by a simple summation over the bending characteristics of the constituent segments.

To formulate a stochastic model for the bending behaviour of an individual segment, we refer to the statistical analysis of DDD curves as demonstrated in the previous section. In stress control, the bending curve of a segment can, above an initial yield stress $\sigma_y$, be envisaged as a stochastic sequence of strain bursts alternating with quasi-elastic loading intervals. Strain burst sizes (plastic surface strain increments) are distributed according to a truncated power law with size-dependent cut-off, Eq. (6), where we identify $l$ with the rod diameter $d$. Strain bursts are separated by stress increments for which we assume a Weibull distribution with exponent $\beta$=1 (i.e., an exponential distribution). The characteristic stress increment $\Delta\sigma_0$ must fulfill the consistency condition $\langle\Delta\sigma\rangle=\Theta\langle\Delta\varepsilon\rangle$ among hardening rate, mean stress, and mean strain increment. This yields with Eqs. (2), (4), and (6) the value $\Delta\sigma_0=(\Theta E\Delta\varepsilon_{\min}b/d)^{1/2}$. Here $\Delta\varepsilon_{\min}$ is a small cut-off strain that is formally required to regularise the non-integrable singularity of the probability distribution (6) at $\Delta\varepsilon\to0$. In the limit of a sufficiently small $\Delta\varepsilon_{\min}$, the particular choice of this parameter does not affect the simulation results. For simplicity, the hardening rate $\Theta$ is assumed to be strain independent (for simulations with strain-dependent $\Theta$, see, e.g., [23]). Thus, the stress-strain curve of each element consists of an elastic part with slope $E$ up to a stress of $\sigma_y$, followed by a random staircase of average slope $\Theta$.

Using this stochastic model for the response of an individual segment, bending simulations are conducted as follows: after dividing the rod of length $L$ into $N=L/d$ segments of length $l=d$ and setting the flow stress for each segment equal to the initial value $\sigma_y$, we execute an iterative Monte Carlo scheme consisting of the following steps:

- Define the active segment $k$ as the segment with the lowest flow stress (if multiple segments have the same flow stress, choose one of them at random).
- Set the scaled bending moment equal to the flow stress $\sigma_k$ of the active segment.
- Increase the bending strain $\varepsilon_k$ of the active segment by a random amount $\Delta\varepsilon$ drawn from distribution (6).
- Increase the flow stress of the active segment by a random amount $\Delta\sigma$ drawn from distribution (2) with parameters as discussed above.
- Evaluate the overall shape of the rod using the relation $\theta_i=\Sigma_{j<i}\varepsilon_j$, where $\theta_j$ is the rotation angle of segment $j$.
- Repeat until the last segment has rotated by 180° ($\theta_N=\pi$).

If we measure stress in units of $E$, the only parameters in the simulations are the scaled specimen diameter $d/b$, the scaled length $N=L/d$, and the scaled hardening rate $\Theta/E$. In the following, we consider specimens of aspect ratio 1:50 ($N$=50), keep the hardening rate at the fixed value $\Theta/E=10^{-3}$, assume a Burgers vector length $b=2.5\times10^{-10}$ m, and vary the specimen diameter $d$ from 100 μm down to 0.1 μm.

Bending shapes and local bending strains resulting from individual simulations are shown in Figure 13. For rod diameters well above 1 μm, bending occurs (apart from boundary effects) in a homogeneous manner, leading to well-controlled circular shapes. At a diameter of 1 μm, on the other hand, and much more so at 0.1 μm, we observe very irregular shapes that differ significantly from the

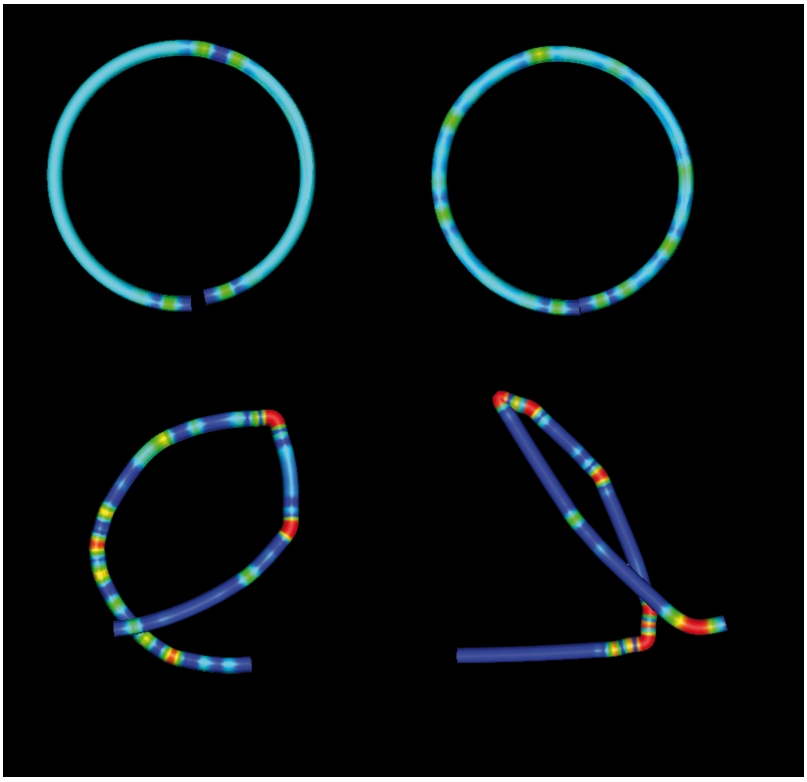

**Figure 13** Results of simulated microbending experiments showing individual outcomes.
Rod diameter: top left, $d$=100 μm; top right, $d$=10 μm; bottom left, $d$=1 μm; bottom right, $d$=0.1 μm.

deterministic expectation. In mathematical terms, this increasing irregularity is related to the fact that the extrinsic cut-off in distribution (6) becomes so large that the maximum strain increment that might be expected from the distribution is not actually reached during the simulation. Our end condition imposes an "extrinsic" cut-off to the strain increment distribution of $\Delta\varepsilon_{max}<\pi$. Using Eq. (6) with $M$=0 and the other parameters as given above, we find that the intrinsic cut-off reaches this value for $d$<0.1 μm. Below this scale, we see "pure" power law statistics. The power law with exponent <2, however, has the property that the strain carried by the largest events makes up an appreciable fraction of the cumulative deformation produced by the ensemble of all strain increments. In simple words, most of the deformation becomes localised in just one or two segments of the rod.

To analyse the spectrum of possible outcomes of our deformation simulations in more quantitative terms, we resort to ensemble simulations and superimpose the outcomes of large numbers of runs to obtain a "density of shapes". Owing to the numerical efficiency of the Monte Carlo scheme, it is not a problem to perform some $10^4$ or $10^5$ runs using the common boundary condition of one end of the rod clamped horizontally in the origin. The resulting spatial density of shapes can be envisaged as the probability that a rod that has been bent using the above scheme with this boundary condition passes through a given point in space. It can thus be used as a measure to quantify shape control for the stochastic microdeformation process. For instance, from this density, we may directly determine the risk that bent parts may pass through or get in contact with undesirable locations. The application, e.g., in shape control of wire bonds is straightforward.

Figure 14 shows the results of ensemble simulations using the same parameters as given above. As above, there is a critical size of about 0.1 μm, below which the resulting shape is entirely controlled by scale-free fluctuations, and as a result, the deformation shapes cannot be controlled at all. Above this scale, however, fluctuations tend to average out with increasing size, leading to a well-defined circular shape in the limit of large rod sizes.

## 5 Summary and conclusions

We have demonstrated how systematic statistical analysis of microdeformation experiments and discrete dislocation dynamics simulations can provide data that serve to

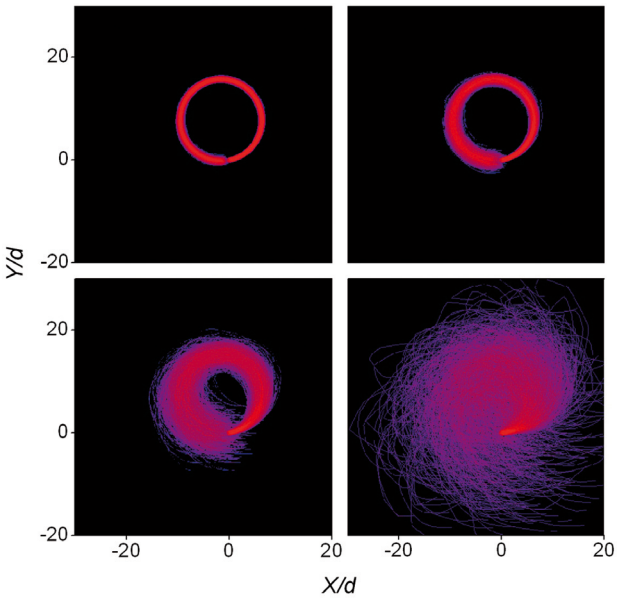


**Figure 14** Each graph represents an ensemble of $10^4$ simulated microbending experiments illustrating the probabilistic spectrum of possible outcomes for different thickness of the bending beams. Top left, $d$=100 μm; top right, $d$=10 μm; bottom left, $d$=1 μm; bottom right, $d$=0.1 μm; in the simulations, one end of the beams is clamped horizontally in the origin while a monotonically increasing torque is applied to the other end.

construct stochastic models that allow the computationally efficient simulation of large ensembles of microdeformation processes. This, in turn, gives access to statistical signatures such as shape densities that allow to assess the spectrum of possible outcomes resulting from the inherently stochastic nature of plasticity on submicrometer scales.

The investigations that we have presented are only a first step on the path towards a comprehensive statistical model of microplasticity. Our example in Section 4 was constructed in such a manner that interactions between different volume elements (rod segments) could be neglected. Thus, information from discrete dislocation dynamics simulations of the bending of short rods could be directly used in constructing the stochastic rules governing deformation of the individual segments of a long rod. In general, however, both long- and short-range interactions between different volume elements need to be considered, and as a consequence, the stress-strain response of a volume element that is part of a larger sample may not be identical – not even in a statistical sense – with the behaviour of the same volume element tested in isolation.

Thus, a more thorough statistical analysis that considers, in addition to the overall stress-strain behaviour of experimental or simulated samples, the plastic response of embedded subvolumes is needed. This is relatively straightforward for dislocation dynamics simulations, which give full access to the internal stress and strain fields above the atomic scale. In the experiment, however, recourse to sophisticated experimental techniques such as microstrain mapping and X-ray microscopy is needed to gain access to internal stress and strain patterns on the micrometer scale. The ultimate aim of such investigations is to understand how the statistical deformation properties of material volumes and subvolumes change as we change the scale of observation and how these changes relate to the characteristic scales of the defect microstructure. As a plastically deforming crystal may be considered as a driven non-equilibrium system in a state close to criticality [20], a study of the scale dependence of fluctuation properties in such systems is tantamount to a renormalisation theory of dislocation plasticity. From a practical point of view, such a theory will help to develop stochastic models that give access to the statistical properties of deformation processes in general geometries and thus pave the way for a comprehensive approach towards computational prediction and control of statistical aspects of microplasticity.

## References

[1] Schneider AS, Clark BG, Frick CP, Gruber PA, Arzt E. *Mater. Sci. Eng. A* 2009, 508, 241–246.
[2] Zaiser M, Schwerdtfeger J, Schneider AS, Frick CP, Clark BG, Gruber PA. *Philos. Mag.* 2008, 88, 3861–3874.
[3] Hollang L, Brunner D, Seeger A. *Mater. Sci. Eng. A* 2000, 319, 233–236.
[4] Uchic MD, Shade PA, Dimiduk D. *Annu. Rev. Mater. Res.* 2009, 40, 361–386.
[5] Kraft O, Gruber PA, Mönig R, Weygand D. *Annu. Rev. Mater. Res.* 2010, 40, 293–317.
[6] Greer JR, De Hosson JTM. *Prog. Mater. Sci.* 2011, 56, 654–724.
[7] Aifantis EC. *Trans. ASME J. Eng. Mater. Technol.* 1984, 106, 326–330.
[8] Fleck NA, Hutchinson JW. *Adv. Appl. Mech.* 1997, 33, 295–361.
[9] Gurtin ME. *J. Mech. Phys. Solids* 2000, 48, 989–1036.
[10] El-Azab A. *Phys. Rev. B* 2000, 61, 11956–11966.
[11] Acharya A. *J. Mech. Phys. Solids* 2004, 52, 301–316.
[12] Hochrainer T, Zaiser M, Gumbsch P. *Philos. Mag.* 2007, 87, 1261–1282.
[13] Zaiser M, Nikitas N, Hochrainer T, Aifantis EC. *Philos. Mag.* 2007, 87, 1283–1306.

[14] Sandfeld S, Hochrainer T, Gumbsch P, Zaiser M. *Philos. Mag.* 2010, 90, 3697–3728.
[15] Sandfeld S, Hochrainer T, Zaiser M, Gumbsch P. *J. Mater. Res.* 2011, 26, 623–632.
[16] Devincre B, Kubin LP, Lemarchand C, Madec R. *Mater. Sci. Eng. A* 2001, 309–310, 211–219.
[17] Weygand D, Friedman LH, van der Giessen E, Needleman A. *Mod. Sim. Mat. Sci. Eng.* 2002, 10, 437–468.
[18] Arsenlis A, Cai W, Tang M, Rhee M, Oppelstrup T, Hommes G, Pierce TG, Bulatov VV. *Mod. Sim. Mat. Sci. Eng.* 2007, 15, 553.
[19] El-Awady JA, Biner SB, Ghoniem NM. *J. Mech. Phys. Solids* 2007, 56, 2019–2035.
[20] Zaiser M. *Adv. Phys.* 2006, 54, 185–245.
[21] Zaiser M, Madani F, Koutsos V, Aifantis EC. *Phys. Rev. Lett.* 2004, 93, 195507.
[22] Schwerdtfeger J, Nadgorny E, Madani-Grasset F, Koutsos V, Blackford JR, Zaiser M. *J. Stat. Mech.* 2007, L04001, 1–8.
[23] Schwerdtfeger J, Nadgorny E, Koutsos V, Blackford JR, Zaiser M. *Acta Mater.* 2010, 58, 4859–4870.
[24] Motz C, Weygand D, Senger J, Gumbsch P. *Acta Mater.* 2008, 56, 1942–1955.
[25] Csikor FF, Motz C, Weygand D, Zaiser M, Zapperi S. *Science* 2007, 318, 251–254.
[26] Zaiser M, Nikitas N. *J. Stat. Mech.* 2007, P04013.
[27] Salman OU, Truskinovsky L. *Phys. Rev. Lett.* 2011, 106, 1–4.
[28] Zaiser M, Aifantis EC. *J. Mech. Behav. Mater.* 2003, 14, 255–270.
[29] Zaiser M, Aifantis EC. *Int. J. Plastic.* 2006, 22, 1432–1455.